Prediction and Observation of Crystal Structures of Oppositely Charged Colloids

A.-P. Hynninen,[1,*] C. G. Christova,[1] R. van Roij,[2] A. van Blaaderen,[1] and M. Dijkstra[1]

[1]*Soft Condensed Matter Group, Department of Physics and Astronomy, Faculty of Science, Utrecht University, Princetonplein 5, 3584 CC Utrecht, The Netherlands*

[2]*Institute for Theoretical Physics, Utrecht University, Leuvenlaan 4, 3584 CE Utrecht, The Netherlands*

(Received 15 July 2005; published 7 April 2006)

We studied crystal structures in mixtures of large and small oppositely charged spherical colloids with size ratio 0.31 using Monte Carlo simulations and confocal microscopy. We developed an interactive method based on simulated annealing to predict new binary crystal structures with stoichiometries from 1 to 8. Employing these structures in Madelung energy calculations using a screened Coulomb potential, we constructed a ground-state phase diagram, which shows a remarkably rich variety of crystals. Our phase diagram displays colloidal analogs of simple-salt structures and of the doped fullerene C_{60} structures, but also novel structures that do not have an atomic or molecular analog. We found three of the predicted structures experimentally, which provides confidence that our method yields reliable results.

DOI: 10.1103/PhysRevLett.96.138308 PACS numbers: 82.70.Dd, 61.50.Ah

Colloidal dispersions consist of nanometer to micrometer sized particles suspended in a solvent. Colloids are important model systems for atoms and molecules, as they exhibit the same phase behavior, but are easier to investigate and to manipulate. The possibility to tune colloidal interactions chemically or by an external field has led to a great variety of model systems. Recently, our group and others presented a new model system, consisting of oppositely charged colloids that form equilibrium crystals [1,2]. A profound difference with atomic systems is that ionic colloidal crystal structures are not dictated by charge neutrality as the charge balance is covered by the presence of counterions. This severs the link between charge ratio and stoichiometry and enlarges the number of possible crystal structures. Predicting these is a computational challenge, not only because of the overwhelming number of possible structures and system parameters (charge, size, solvent, salinity, composition, etc.) but also because of the intricate interplay between attractive and repulsive interactions, entropy, and packing effects. In this Letter, we develop a novel interactive simulation method to predict binary crystal structures of oppositely charged colloids, based on simulated annealing [3]. Employing this method, we are able to predict a whole variety of new binary crystal structures with different stoichiometries, which we used in Madelung energy calculations to map out the ground-state phase diagram. Results are presented for binary mixtures of small and large oppositely charged colloids with size ratio 0.31, corresponding to one of our experimental systems that triggered our theoretical interest [1]. The calculated phase diagram exhibits a plethora of different crystal structures, some of which have atomic and molecular analogs, while others do not. Using the theoretical predictions, we experimentally confirmed the stability of three of the crystal structures.

Our experimental system consists of spherical, sterically stabilized polymethylmethacrylate (PMMA) particles [4], dispersed in a less polar solvent mixture. The negatively charged larger particles have a radius $a_L = 1.16\ \mu$m (polydispersity 3%), and the positively charged smaller particles have a radius $a_S = 0.36\ \mu$m (polydispersity 5%); hence, the size ratio is $a_S/a_L = 0.31$. The large spheres are labeled with rhodamine isothiocyanate and the small ones with 7 nitrobenzo-2 oxa-1,3 diazol, by which they can be distinguished using fluorescence microscopy. The colloids are dispersed in a density and refractive index matching mixture of cyclohexylbromide-decalin (80/20 volume ratio). This, together with sterical stabilization, minimizes the van der Waals forces. The preparation of the binary mixtures and samples is described in Ref. [1]. Image analysis of xyz data stacks obtained by confocal scanning laser microscopy allows the structures to be studied in real space.

We model this system as N_L large colloids in a volume V with a radius a_L carrying a negative charge $Z_L e$ (where $Z_L < 0$ and e is the proton charge) and N_S small colloids with a radius a_S carrying a positive charge $Z_S e$ ($Z_S < |Z_L|$). We assume that the pair potential $u_{ij}(r)$, between colloid i and j at interparticle separation r, is given by an approximate solution of the Poisson-Boltzmann theory [5]

$$\frac{u_{ij}(r)}{k_B T} = \begin{cases} \frac{Z_i Z_j \lambda_B e^{\kappa(a_i+a_j)}}{(1+\kappa a_i)(1+\kappa a_j)} \frac{e^{-\kappa r}}{r}, & r \geq a_i + a_j, \\ \infty, & r < a_i + a_j, \end{cases} \quad (1)$$

where Z_i (Z_j) and a_i (a_j) are the charge number and radius of colloid i (j), $\lambda_B = e^2/\epsilon_s k_B T$ is the Bjerrum length, $\kappa = \sqrt{8\pi\lambda_B \rho_{\text{salt}}}$ is the inverse Debye screening length, ϵ_s is the dielectric constant of the solvent, and ρ_{salt} is the salt concentration. The potential in Eq. (1) is one of the simplest ways to model interactions between oppositely charged colloids. It has been shown to give a good description at small κ [6] and is known to work for same charged colloids. We denote the composition by $x = N_S/(N_L + N_S)$, the packing fraction of large colloids by $\eta_L = 4\pi a_L^3 N_L/3V$, the dimensionless large-small-colloid contact potential by $\Gamma = |u_{LS}(a_L + a_S)|/k_B T$, and the charge

ratio by $Q = |Z_L/Z_S|$. We fix the size ratio to the experimental value $a_S/a_L = 0.31$.

Binary crystal structure candidates were predicted using an interactive Monte Carlo (MC) simulation program. The simulations are performed using periodic boundary conditions. The program has real-time visualization and allows us to change various parameters (Γ, Q, κ, stoichiometry) during the simulation, to switch between constant pressure (NPT) and canonical (NVT) ensembles [7], and to turn on (or off) large-colloid displacement moves. The simulations were started in the NVT ensemble with the large colloids in a face-centered-cubic (fcc), body-centered-cubic (bcc), hexagonal-close-packed (hcp), simple cubic (sc), simple hexagonal (sh) ,or base-centered (bc) crystal and the small colloids at random (nonoverlapping) positions. Next we used simulated annealing to increase Γ slowly from 0 (high temperatures) to $\Gamma \approx 10$–20 (which gives us the ground-state structure), while only the small colloids were allowed to move. At the final Γ, we switch to the NPT ensemble, where volume moves were performed separately for each axis in order to equilibrate the small-colloid positions and the box shape. Finally, the large-colloid moves were turned on and the ideal crystal structures were constructed from snapshots of the final colloid configuration.

The search for new stable binary structures was performed by trying all the above mentioned large-colloid crystals as starting configurations, at packing fractions around $\eta_L = 0.3$–0.56 and at various initial shapes of the simulation box. This was repeated for small-large stoichiometries $n = 1$–8 (denoted by LS_n), where $n = x/(1-x)$. The simulations were performed with 4–16 large colloids. A small simulation box with periodic boundaries facilitates finding structures with crystalline order, as it reduces the probability of stacking faults. Table I lists the crystal structures found for each stoichiometry and large-colloid starting configuration, for $\kappa a_L = 2$ and $Q = n$. Structures with no atomic or molecular analog are named LS_n^{lat}, where ''lat'' is the lattice symmetry of the large colloids. In the colloidal analogs of the fullerene structures A_4C_{60} [8] and body-centered-cubic A_6C_{60} (or $A_6C_{60}^{\mathrm{bcc}}$) [9], the large colloids correspond to C_{60} and the small ones to A (= K, Rb, or Cs). We have not considered primitive unit cells with more than two large colloids and have hence excluded structures with $n = 5$ and 7, as well as some other structures (e.g., the face-centered-cubic A_6C_{60} structure [10]). This does not mean that these structures could not form in experiments.

TABLE I. The crystal structures found with simulated annealing for each large-colloid starting configuration and stoichiometry n. C_{60} stands for the fullerene molecule and a line (—) indicates the absence of crystal structure.

LS_n	fcc	bcc	sc	sh	hcp	bc
1	Zinc blende	Zinc blende	—	—	wurtzite	—
2	CaF_2	CaF_2	—	—	—	CaF_2
3	LS_3^{fcc}	Cr_3Si	ReO_3	Li_3N	LS_3^{hcp}	ReO_3
4	A_4C_{60}, LS_4^{bct}	A_4C_{60}, SiF_4	—	—	LS_4^{hcp}	—
6	$A_6C_{60}^{\mathrm{bcc}}$, LS_6^{fcc}	$A_6C_{60}^{\mathrm{bcc}}$	—	—	$LS_6^{\mathrm{hcp+hp}}$	—
8	LS_8^{fcc}	LS_8^{fcc}	—	LS_8^{hcp}	LS_8^{hcp}	—

Predicting the phase diagram of a binary mixture often involves a calculation of the Gibbs free energy per particle, since its x dependence at fixed P and T allows for common tangent constructions. It reduces, however, to the enthalpy for the ground-state properties of interest here, where entropic effects are ignored. Moreover, since many of our experiments show crystals that are self-supported by their cohesive energy, we restrict attention to the zero-pressure limit. The present phase diagram follows therefore from the internal energy, which for an ideal crystal is the composition dependent Madelung energy $U(x)$ [1,6]. Including entropy and pressure complicates theoretical studies considerably and will be the subject of future research.

In the zero-pressure ground-state approximation, phase stability depends only on Q, κ, and x and *not* on the absolute values of Z_L, Z_S, and λ_B. We calculated $U(x)$ with the MC code for the structures listed in Table I and for many known structures: NaCl, CsCl, NiAs, CuAu, AlB_2, Cu_3Au, Al_3Ti, $CaCu_5$, and CaB_6 [11]. The lowest $U(x)$ per colloidal particle was found for given Q and κ by optimizing each possible structure with respect to η_L and the shape of the unit cell. We then performed the common tangent construction to obtain the three-dimensional (Q, κ, x) phase diagram. Figures 1(a) and 1(b) show the resulting $(Q, \kappa a_L)$ planes of the phase diagram for fixed composition (a) $x = 1^-$ and (b) $x = 0^+$, corresponding to crystal structures coexisting with an infinitely dilute gas of pure small colloids, and of pure large colloids, respectively. Figure 1(c) plots the (Q, x) plane for fixed $\kappa a_L = 2.5$ and shows crystal-crystal phase coexistence for $0 < x < 1$.

Figure 1 shows an increasing stoichiometry with increasing Q at low κa_L. In addition, one observes that an excess of small colloids favors structures with high stoichiometry. Moreover, we see that ReO_3, Li_3N, SiF_4, LS_6^{fcc}, and LS_6^{hcp} are stable only for relatively long-ranged interactions with $\kappa a_L \sim 0.5$. In these structures, shown in Figs. 2(a)–2(e), the small colloids are in between pairs of neighboring large colloids in the sc (ReO_3), sh (Li_3N), bcc (SiF_4), fcc (LS_6^{fcc}), or hcp (LS_6^{hp}) structure. At small κ, salt partitioning is important and should be taken into account. However, using parameters relevant to experiments, we estimate that at $\kappa a_L > 1.5$ salt partitioning does not play a major role, and thus the most prominent features of the phase diagram are expected to be correct. At $Q \approx 1$, we find the wurtzite structure; see Fig. 2(f). The CaF_2 structure has the large colloids in an fcc lattice and the small colloids in the tetrahedral holes [Fig. 2(g)]. The Cr_3Si structure has the large colloids in a bcc lattice and the small colloids as shown in Fig. 2(h). LS_6^{hp}, shown in

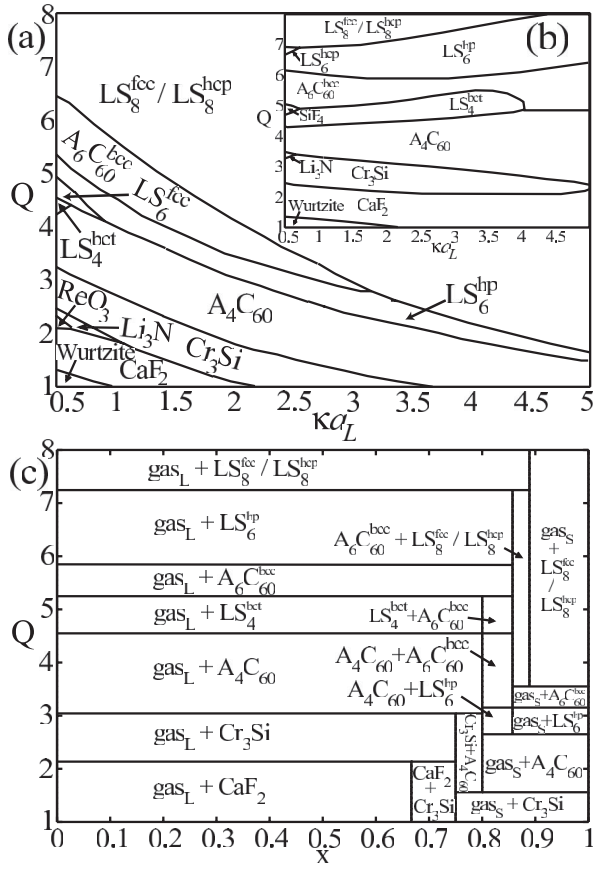

FIG. 1. The ground-state phase diagram of a mixture of large and small oppositely charged colloids with size ratio 0.31: (a) and (b), as a function of the Debye screening parameter κ and the charge ratio Q, and (c), as a function of composition x and Q for $\kappa a_L = 2.5$. In (a), the structures coexist with a gas of pure small colloids, and in (b) with one of large colloids. In (c), "gas_L" and "gas_S" refer to gas of large and small colloids, respectively. Note that the path $\kappa a_L = 2.5$ in (a) and (b) corresponds to the coexisting crystals at $x = 1^-$ and $x = 0^+$ in (c), respectively.

Fig. 2(i), consists of hexagonal planes of large colloids, which are slightly compressed (6%–10%) with respect to an ideal hcp crystal, and of small colloids, which are in two kagome patterns [12] above and below each large-colloid hexagonal layer. In the A_4C_{60} structure [8], the large colloids are in a body-centered-tetragonal (bct) lattice, and the small colloids are between two large colloids such that they form a square parallel to the square plane of the tetragonal unit cell; see Fig. 2(j). The LS_4^{bct} structure, shown in Fig. 2(k), differs from A_4C_{60} in that the small colloids are turned 45° in the square plane.

To verify the theoretical phase diagram, we studied the crystal structures and their formation in our experimental system, with total particle volume fraction 0.2 and added salt (tetrabutylammonium bromide) concentrations in the range 15–35 μM. Interestingly, we experimentally found three of the predicted crystal structures, viz. $A_6C_{60}^{\text{bcc}}$, LS_8^{fcc}, and LS_8^{hcp}, which are indeed rather dominant in the phase

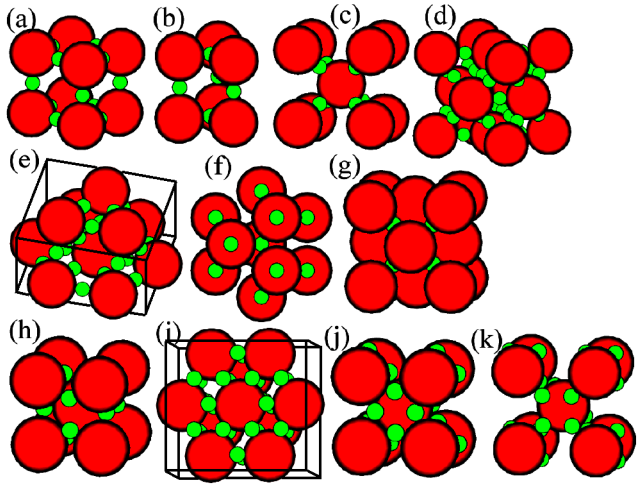

FIG. 2 (color online). Theoretically predicted stable binary crystal structures: (a) ReO_3, (b) Li_3N, (c) SiF_4, (d) LS_6^{fcc}, (e) LS_6^{hcp}, (f) wurtzite, (g) CaF_2, (h) Cr_3Si, (i) LS_6^{hp}, (j) A_4C_{60}, and (k) LS_4^{bct}.

diagram of Fig. 1 at large Q. Typically, crystal nuclei appeared within 24 h after preparation of the samples (the earliest were observed after 4–5 h). They had different orientations, which suggests homogeneous nucleation. With time, the crystal domains grew larger and reached sizes of about 100 μm. In the LS_8^{hcp} structure, the large colloids form an hcp lattice. In the hexagonal layers, each large colloid is surrounded by a ring of 6 small ones occupying the trigonal interstices. Above and below each layer, there are two planes of small colloids ordered in a kagome pattern; see Fig. 3(a). Figure 3(b) shows the LS_8^{hcp} structure as a superposition of 5 layers of large colloids and 15 layers of small colloids. In the LS_8^{fcc} crystal, the large colloids are ordered in an fcc lattice, and in every octahedral hole there are 8 small colloids forming a cube; see Fig. 3(c). Figure 3(d) shows the (100) plane of the LS_8^{fcc} unit cell, and in Fig. 3(e), the (110) plane is shown. The insets in Figs. 3(d) and 3(e) show the corresponding planes of this structure predicted by our simulations, revealing excellent agreement. Experimentally, the LS_8^{hcp} and LS_8^{fcc} structures were found to coexist. This is also in agreement with our calculations, which predict essentially equal Madelung energies (LS_8^{fcc} is more stable, but only by 0.005%–0.1%). The $A_6C_{60}^{\text{bcc}}$ structure [9] consists of a bcc lattice of the large colloids with 4 small colloids in a square situated in the plane between every large next nearest neighbor; see Fig. 3(f). Figures 3(g) and 3(h) show, respectively, the (100) and (110) planes of the $A_6C_{60}^{\text{bcc}}$ structure unit cell together with the corresponding calculations. Note that this $A_6C_{60}^{\text{bcc}}$ crystal is different from the LS_6 structure observed in Ref. [1]. According to the Madelung energy calculations, $A_6C_{60}^{\text{bcc}}$ (which was not considered in Ref. [1]) is more stable than LS_6. It is

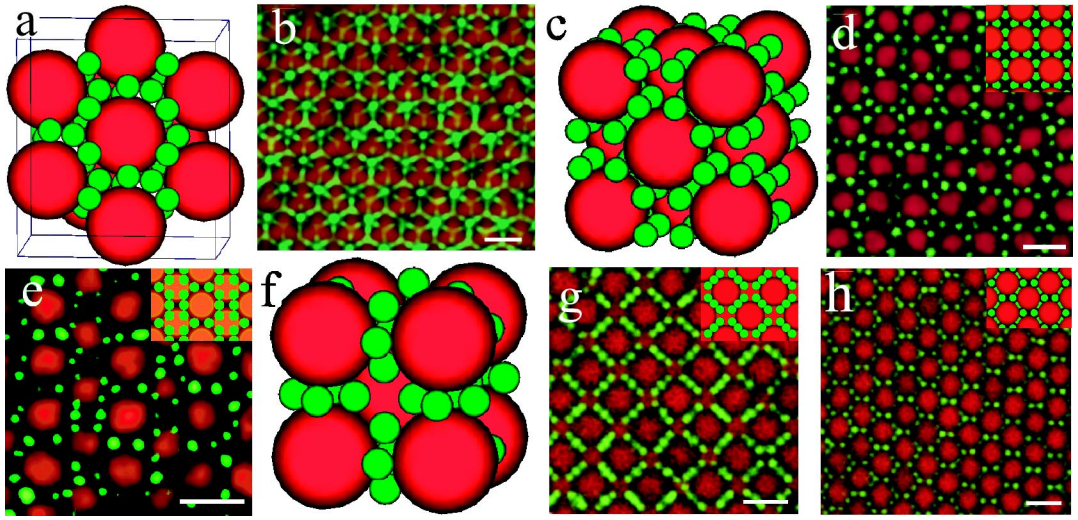

FIG. 3 (color online). Experimental observations and the corresponding theoretical predictions of binary structures. Confocal images of small positive light (green) and large negative dark (red) PMMA particles: (b) superposition of several layers of LS_8^{hcp}; (d) (100) plane of LS_8^{fcc}; (e) (110) plane of LS_8^{fcc}; (g) (100) plane of $A_6C_{60}^{\mathrm{bcc}}$; (h) (110) plane of $A_6C_{60}^{\mathrm{bcc}}$. All scale bars are 3 μm. The insets in (d), (e), (g), and (h) show the corresponding plane in the theoretical predictions. Unit cells of (a) LS_8^{hcp}, (c) LS_8^{fcc}, and (f) $A_6C_{60}^{\mathrm{bcc}}$ structures.

possible, though, that entropy and pressure can change the relative stability of these two structures.

In conclusion, we have developed an interactive method based on simulated annealing to predict binary crystal structures of oppositely charged colloids, from which we constructed a ground-state phase diagram for size ratio 0.31. Our phase diagram displays novel structures but also colloidal analogs of simple-salt structures and of doped fullerene C_{60} structures. The latter is not surprising as the size ratios of the two systems are very similar, e.g., $a_{\mathrm{Rb}}/a_{C_{60}} = 0.3$. Three of the predicted structures, $A_6C_{60}^{\mathrm{bcc}}$, LS_8^{fcc}, and LS_8^{hcp}, were also observed experimentally, thereby providing confidence that the proposed method with the screened Coulomb potential yields reliable predictions, although the experimentally observed Brownian motion suggests that entropy should not be ignored. We have so far restricted our attention to stoichiometries up to $n = 8$ but expect more structures for larger n; e.g., for $n = 10$ and $Q \approx 10$, we expect a colloidal analog of the $Na_{10}C_{60}$ structure [13]. It is possible that other structures exist that make the current ones metastable. However, introduction of a new structure typically reduces the stability area of the prior ones but does not completely replace them. It is interesting to compare our method for finding new structures with genetic algorithms [14]. Finally, it is reasonable to expect even more and different structures for other size ratios, the exploration of which is not only of fundamental but also of practical interest, e.g., for photonic applications.

We thank E. C. M. Vermolen, M. E. Leunissen, and P. N. Pusey for useful discussions. This work is part of the research program of the "Stichting voor Fundamenteel Onderzoek der Materie (FOM)," which is financially supported by the "Nederlandse Organisatie voor Wetenschappelijk Onderzoek (NWO)."

*Present address: Department of Chemical Engineering, Princeton University, Princeton, NJ 08544, USA.

[1] M. E. Leunissen *et al.*, Nature (London) **437**, 235 (2005).
[2] P. Bartlett and A. I. Campbell, Phys. Rev. Lett. **95**, 128302 (2005).
[3] S. Kirkpatrick *et al.*, Science **220**, 671 (1983).
[4] G. Bosma *et al.*, J. Colloid Interface Sci. **245**, 292 (2002).
[5] B. Derjaguin and L. Landau, Acta Physicochim URSS **14**, 633 (1941); E. J. W. Verwey and J. Th. G. Overbeek, *Theory of the Stability of Lyotropic Colloids* (Elsevier, Amsterdam, 1948).
[6] G. R. Maskaly, Ph.D. thesis, MIT, Boston, 2005.
[7] D. Frenkel and B. Smit, *Understanding Molecular Simulations* (Academic, New York, 2002), 2nd ed.
[8] R. M. Fleming *et al.*, Nature (London) **352**, 701 (1991).
[9] O. Zhou *et al.*, Nature (London) **351**, 462 (1991).
[10] M. J. Rosseinsky *et al.*, Nature (London) **356**, 416 (1992).
[11] L. Pauling, *The Nature of the Chemical Bond* (Cornell University, Ithaca, New York, 1960), 3rd ed.
[12] K. Husimi and I. Syôzi, Prog. Theor. Phys. **5**, 177 (1950).
[13] T. Yildirim *et al.*, Nature (London) **360**, 568 (1992); L. Forró and L. Mihály, Rep. Prog. Phys. **64**, 649 (2001).
[14] D. M. Deaven and K. M. Ho, Phys. Rev. Lett. **75**, 288 (1995); D. Gottwald *et al.*, J. Chem. Phys. **122**, 204503 (2005).